

Thermoelectricity and electronic correlations enhancement in FeS by slight Se substitution

Yu Liu,^{1,†,‡,*} Aifeng Wang,^{1,||,§,*} V. N. Ivanovski,² Qianheng Du,^{1,3,#} V. Koteski,² and C. Petrovic^{1,3,¶}

¹Condensed Matter Physics and Materials Science Department,
Brookhaven National Laboratory, Upton, New York 11973, USA

²Department of Nuclear and Plasma physics, Vinca Institute of Nuclear Sciences -
National Institute of the Republic of Serbia, University of Belgrade, Belgrade, Serbia

³Department of Materials Science and Chemical Engineering,
Stony Brook University, Stony Brook, New York 11790, USA

(Dated: March 1, 2022)

We report thermoelectric studies of $\text{FeS}_{1-x}\text{Se}_x$ ($x = 0, 0.06$) superconducting single crystals that feature high irreversibility fields and critical current density J_c comparable to materials with much higher superconducting critical temperatures (T_c 's). The ratio of T_c to the Fermi temperature T_F is very small indicating weak electronic correlations. With a slight selenium substitution on sulfur site in FeS both T_c/T_F and the effective mass m^* rise considerably, implying increase in electronic correlation of the bulk conducting states. The first-principle calculations show rise of the density of states at the Fermi level in $\text{FeS}_{0.94}\text{Se}_{0.06}$ when compared to FeS which is related not only to Fe but also to chalcogen-derived electronic states.

INTRODUCTION

Since the discovery of $\text{La}(\text{O}_{1-x}\text{F}_x)\text{FeAs}$ ($x = 0.05-0.12$) with a superconducting transition temperature $T_c = 26$ K [1], the layered iron-based superconductors have been extensively studied. Stoichiometric tetragonal FeS showing a T_c below 5 K was synthesized in 2015 by using a hydrothermal method [2]. It shares the same simplest PbO-type structure with FeSe [3], which motivated many subsequent studies devoted to investigation of its superconducting state and relation to crystal structure details.

In contrast to FeSe, the X-ray diffraction experiment indicated no structural transition down to 10 K in FeS [4, 5]. The T_c of FeS continuously decreases for hydrostatic pressures up to 2.2 GPa [6], while a second superconducting dome for higher pressures from 5 to 22.3 GPa has been observed with an enhanced T_c [7]. The neutron scattering experiment and angle-resolved photoemission spectroscopy (ARPES) measurement indicated that FeS is less correlated when compared to FeSe [8, 9], however the scanning tunneling microscopy (STM) measurement suggested a strong-coupling superconductivity with a large gap ratio of ~ 4.65 in FeS [10]. The thermal conductivity and heat capacity measurements suggested a nodal or highly anisotropic superconducting gap structure in FeS [11, 12], while a μSR study proposed that a full-gap state coexists with low-moment disordered magnetism [6]. A large upper critical field anisotropy $H_{c2}^{\parallel ab}(0)/H_{c2}^{\parallel c}(0) = 10$ has been observed in angle-dependent magnetoresistance and quantum oscillations, in line with the band structure calculation [13–16]. The nonlinear behavior of Hall resistivity indicated multiband conductivity [15]. Interestingly, the critical current density J_c in FeS is comparable to other iron-based superconductors with much higher T_c , and it can be enhanced three times by 6% Se doping [17, 18], point-

ing that FeS-based materials with higher T_c are promising for high-magnetic-field applications.

Thermopower is an effective parameter to characterize the nature and sign of carries as well as the correlation strength in superconductors [19–27]. Fundamentally, the thermopower is entropy per carrier. To evaluate the correlation strength of electronic states in the bulk that may influence anisotropy of both normal state and the J_c as well as the current-carrying capability in grain boundaries [28–33], in this work we perform thermal transport studies of superconducting $\text{FeS}_{1-x}\text{Se}_x$ ($x = 0$ and 0.06) single crystals. The Fermi temperature T_F in both crystals is about an order of magnitude smaller when compared to common values in metals. Rather small T_c/T_F suggests weak electronic correlations. Yet, our combined experimental and theoretical analysis indicates an increase of electronic correlations for a change in x as small as 0.06, i.e. in $\text{FeS}_{0.94}\text{Se}_{0.06}$ when compared to FeS.

EXPERIMENTAL DETAILS

Single crystals of $\text{FeS}_{1-x}\text{Se}_x$ ($x = 0, 0.06$) were synthesized by a hydrothermal method and characterized as described previously [17, 18]. X-ray diffraction (XRD) data were acquired on a Rigaku Miniflex powder diffractometer with $\text{Cu } K_\alpha$ ($\lambda = 0.15418$ nm). The in-plane resistivity ρ and thermopower S were measured in a Quantum Design PPMS-9 system with standard four-probe technique. Thermopower was measured by using one-heater-two-thermometer setup with hooked copper leads using silver paint contact directly on crystals with typical dimensions $\sim 4 \times 3 \times 0.3$ mm³. Continuous measuring mode was adopted for thermopower measurement with the maximum heater power and period set as 50 mW and

1430 s along with the maximum temperature rise of 3%. The relative error in our measurement for thermopower was below 5% based on Ni standard measured under identical conditions. The Hall resistivity ρ_{xy} was measured using standard four-probe method with the current flowing in the ab plane and the magnetic field along the c axis. In order to effectively eliminate the longitudinal resistivity contribution due to voltage probe misalignment, the Hall resistivity was obtained by the difference of transverse resistance measured at positive and negative fields, i.e. $\rho_{xy} = [\rho(+\mu_0 H) - \rho(-\mu_0 H)]/2$. The sample dimensions were measured by an optical microscope Nikon SMZ-800 with 10 μm resolution. The heat capacity was measured on warming procedure between 0.35 and 7 K by the heat pulse relaxation method in a Quantum Design PPMS-9.

The density of states of both FeS and $\text{Fe}_{16}\text{S}_{15}\text{Se}_1$ were calculated by the VASP code in the gradient corrected (GGA) implementation [34] using the experimental value of FeS lattice parameter c . Lattice parameter a and internal parameter u were DFT-relaxed. The non-magnetic ground states were obtained via the Methfessel-Paxton order 1 integration method of the Brillouin zone using a grid of $13 \times 13 \times 9$ k -points. The maximum forces are less than 0.02 eV \AA^{-1} and the energy criterion was set to 10^{-5} eV.

RESULTS AND DISCUSSIONS

Figure 1(a) shows the single crystal XRD patterns of tetragonal $\text{FeS}_{1-x}\text{Se}_x$ ($x = 0$ and 0.06). Only (001) reflections were observed for both crystals, yielding the c -axis lattice parameter $c = 5.035(5)$ and $5.061(22)$ \AA for FeS and $\text{FeS}_{0.94}\text{Se}_{0.06}$, respectively. The crystal structure as presented in the inset in Fig. 1(a); it is composed of a stack of edge-sharing FeS_4 tetrahedra layer by layer, without a spacer layer [2]. The FeS_4 tetrahedron is nearly regular with two S-Fe-S angles very close to the ideal value of 109.5° [35].

The in-plane resistivity $\rho(T)$ for $\text{FeS}_{1-x}\text{Se}_x$ ($x = 0$ and 0.06) [Fig. 1(b)] monotonically decreases with decreasing temperature showing good metallic conductivity. The residual resistivity ratio $RRR = \rho(300 \text{ K})/\rho(5 \text{ K})$ is ~ 68 for FeS, indicating low defect scattering. The value of RRR decreases to ~ 27 for $\text{FeS}_{0.94}\text{Se}_{0.06}$ with S/Se substitution disorder. The $\rho(T)$ of $\text{FeS}_{1-x}\text{Se}_x$ ($x = 0$ and 0.06) shows a positive curvature all the way up to room temperature, in contrast to FeSe where a negative curvature is generally observed at high temperatures [3]. An abrupt resistivity drop can be clearly seen [Fig. 1(c)], signaling the onset of superconductivity. Zero resistivity is observed at $T_c = 4.5(1)$ K for FeS, in agreement with the previous reports [15]. The T_c is slightly lower with a value of $4.1(1)$ K for $\text{FeS}_{0.94}\text{Se}_{0.06}$.

Figure 2(a) shows the temperature dependence of in-

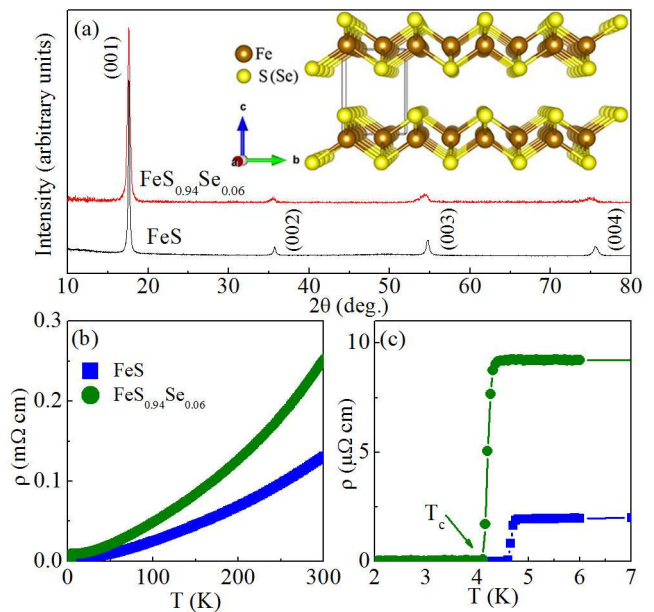


FIG. 1. (Color online) (a) Single crystal X-ray diffraction (XRD) patterns of $\text{FeS}_{1-x}\text{Se}_x$ ($x = 0, 0.06$). Inset shows the crystal structure with the space group $P4/nmm$. (b) Temperature dependence of in-plane resistivity $\rho(T)$ for $\text{FeS}_{1-x}\text{Se}_x$ ($x = 0, 0.06$) single crystals. (c) The enlargement of superconducting transitions at low temperature.

plane thermopower $S(T)$ for $\text{FeS}_{1-x}\text{Se}_x$ ($x = 0$ and 0.06). At room temperature, the $S(T)$ for both samples shows a negative value, consistent with dominant negative charge carriers [15]. It is interesting that the value of $S(T)$ decreases with decreasing temperature and becomes positive at $\sim 122(4)$ and $228(4)$ K for FeS and $\text{FeS}_{0.94}\text{Se}_{0.06}$, respectively. For pure FeS, the positive $S(T)$ gradually increases with a much smaller slope and features a broad peak [$\sim 1.3(2)$ $\mu\text{V K}^{-1}$] around 28(9) K, then decreases again as temperature is lowered. The sign change of $S(T)$ implies multiband transport in FeS, in agreement with the nonlinear Hall resistivity analysis [15]. Even though the Hall coefficient R_H is unchanged in this temperature range [15], the sign of $S(T)$ might change due to a different dependence on the carrier density n_e (n_h), mobility μ_e (μ_h), and S_e (S_h) in the two-band model [36]:

$$R_H = \frac{1}{e} \frac{n_h \mu_h^2 - n_e \mu_e^2}{(n_h \mu_h + n_e \mu_e)^2}, \quad (1)$$

$$S = \frac{S_e n_e \mu_e + S_h n_h \mu_h}{n_e \mu_e + n_h \mu_h}. \quad (2)$$

The positive $S(T)$ of $\text{FeS}_{0.94}\text{Se}_{0.06}$ changes its slope from negative to positive temperature dependence at 107(3) K with a larger maximum value of $7.22(1)$ $\mu\text{V K}^{-1}$. With further decrease in temperature, the $S(T)$ for both samples becomes negative again and vanishes at T_c since the Cooper pairs carry no entropy. The $S(T)$ of FeSe is positive at room temperature of ~ 10 $\mu\text{V K}^{-1}$, then decreases

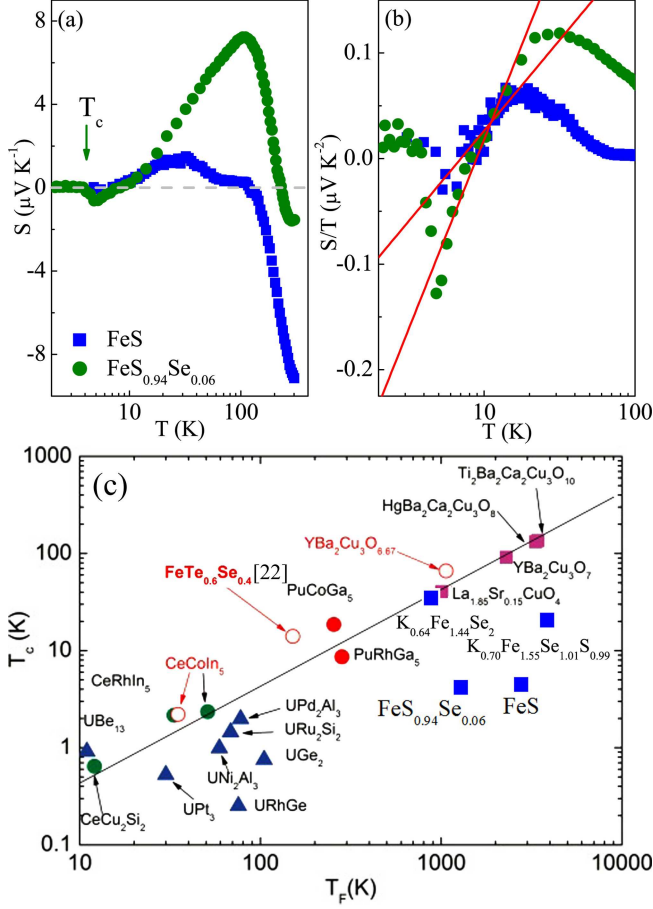


FIG. 2. (Color online) Temperature dependence of in-plane (a) thermopower $S(T)$ and (b) S/T for FeS_{1-x}Se_x ($x = 0$ and 0.06) single crystals. (c) The Moriya-Ueda plot: T_c as a function of T_F for indicated superconductors [22, 45, 46]; Four blue solid squares represent K_{0.64}Fe_{1.44}Se₂, K_{0.70}Fe_{1.55}Se_{1.01}S_{0.99} [26], and FeS_{1-x}Se_x ($x = 0, 0.06$).

with decreasing temperature and changes its sign to be negative below 200 K and back to be positive again near 30 K above T_c , featuring a minimum value of $-10 \sim -15 \mu\text{V K}^{-1}$ around 115 K [37–39]. The similar multiple sign changes in $S(T)$ suggests that almost compensated electrons and holes complete in FeS_{1-x}Se_x. From the band structure calculations [40], indeed, both the hole and electron pockets appear in the identical Fermi-surface area. However, the complex details of $S(T)$ make it difficult to be reproduced by the theory calculation using constant relaxation time approximation [38], calling for further improved method taken into consideration the correlation effects in this system.

Generally, the phonon drag S_{drag} related to electron-phonon coupling gives $\propto T^3$ dependence for $T \ll \Theta_D$, $\propto T^{-1}$ for $T \gg \Theta_D$, and a peak structure at $\sim \Theta_D/5$, where Θ_D is the Debye temperature [41, 42]. The derived Θ_D is about 230 K for FeS [12]. Since there is no peak structure at $\Theta_D/5 = 50.7(1)$ K for FeS and thermopower

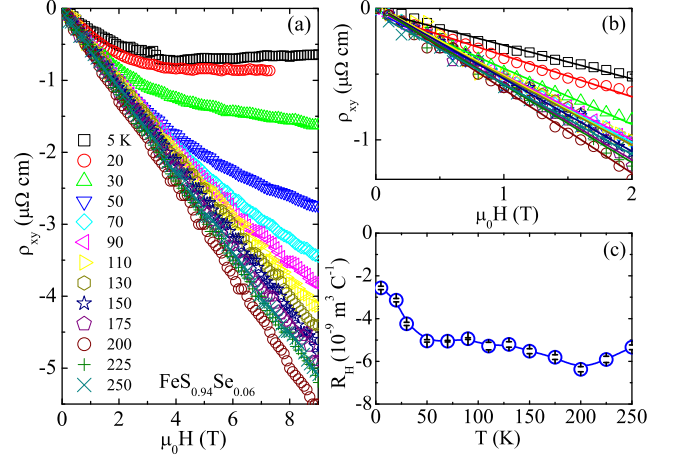


FIG. 3. (a) Field dependence of the Hall resistivity ρ_{xy} for FeS_{0.94}Se_{0.06} at various temperatures. (b) Plots of ρ_{xy} vs $\mu_0 H$ below 2 T with solid linear fitting curves. (c) Temperature dependence of Hall coefficient R_H derived from linear fit in (b) below 2 T.

is linear for FeS_{0.94}Se_{0.06} around 49.1(1) K (see below for the values of Θ_D), it is unlikely that the sign and slope change in $S(T)$ is related to the phonon drag effect.

Figure 2(b) shows the temperature dependent of $S(T)$ divided by temperature for FeS_{1-x}Se_x ($x = 0$ and 0.06). The zero-temperature extrapolated value of S/T increases with Se doping; it is $\sim -0.15(1) \mu\text{V K}^{-2}$ for FeS and reaches $-0.34(3) \mu\text{V K}^{-2}$ for FeS_{0.94}Se_{0.06}, with a magnitude proportional to the strength of electron correlation [43]. The S is usually given by [41, 43, 44],

$$\frac{S}{T} = \pm \frac{\pi^2 k_B}{2} \frac{1}{e T_F} = \pm \frac{\pi^2 k_B^2}{3} \frac{N(\varepsilon_F)}{e n}, \quad (3)$$

where e is the electron charge, k_B is the Boltzmann constant, T_F is the Fermi temperature, which is related to the Fermi energy ε_F and the density of states $N(\varepsilon_F)$ as $N(\varepsilon_F) = 3n/2\varepsilon_F = 3n/k_B T_F$, and n is the carrier concentration (the positive sign is for hole and the negative sign is for electron). In a multiband system, it gives the upper limit of T_F of the dominant band. Therefore we can extract $T_F = 2.8(2) \times 10^3$ K for FeS and $1.25(11) \times 10^3$ K for FeS_{0.94}Se_{0.06}, respectively. The ratio of T_c/T_F characterizes the correlation strength in superconductors. For example, the T_c/T_F is close to 0.1 in Fe_{1+y}Te_{1-x}Se_x [22], pointing to the importance of electronic correlation, while it is ~ 0.02 in BCS superconductor, such as LuNi₂B₂C [22]. The value of T_c/T_F is $\sim 0.0016(1)$ for FeS and $\sim 0.0033(2)$ for FeS_{0.94}Se_{0.06}, indicating weak electronic correlations but also a substantial enhancement for rather small amount of Se substitution on S atomic site. The value of T_c/T_F is also smaller than that of K_xFe_{2-y}Se₂ ~ 0.04 [25], but comparable with that of K_xFe_{2-y}Se_{1-z}S_z ~ 0.005 [26], which are also added into the Moriya-Ueda plot for comparison

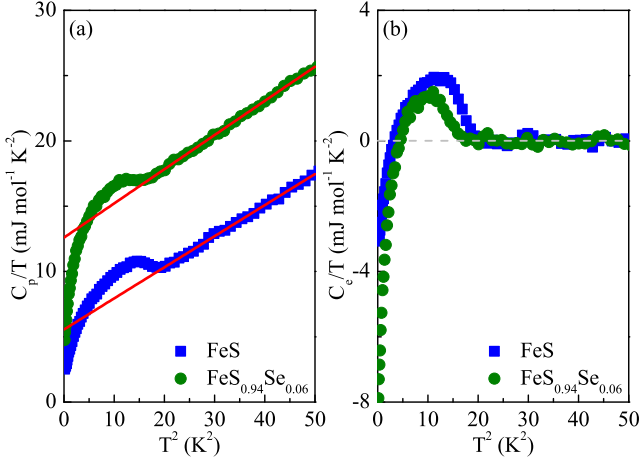


FIG. 4. (a) Temperature dependence of heat capacity C_p/T vs T^2 for for $\text{FeS}_{1-x}\text{Se}_x$ ($x = 0$ and 0.06) single crystals. The solid curve represents the fittings using $C_p/T = \gamma + \beta T^2$. (b) The low temperature electronic part C_e/T vs T^2 in zero field.

[Fig. 2(c)] [22, 45, 46].

Figure 3 shows the Hall resistivity ρ_{xy} of $\text{FeS}_{0.94}\text{Se}_{0.06}$. At low temperatures, the ρ_{xy} shows a nonlinear correlation with the magnetic field, similar to FeS [15], confirming a multiband effect. With increasing temperature, the nonlinear ρ_{xy} gradually evolves to linear at high temperatures (above 110 K). Then we estimated the Hall coefficient R_H by fitting the low field data in Fig. 3(b), and plotted the temperature-dependent R_H in Fig. 3(c). The R_H is negative in the whole temperature range, indicating dominant electron carriers, as well as a nonmonotonic temperature dependence, similar with that in FeS [15].

The temperature-dependent heat capacity C_p/T in the low-temperature range as a function of T^2 in zero magnetic field for $\text{FeS}_{1-x}\text{Se}_x$ ($x = 0, 0.06$) is depicted in Fig. 4(a). A clear specific heat jump is observed at T_c for both samples, in line with the resistivity and thermopower data, indicating bulk superconductivity. The data from 4.5 to 7 K can be well fitted by $C_p/T = \gamma + \beta T^2$ [Fig. 4(a)], where the first term is the Sommerfeld electronic specific heat coefficient, the second term is low-temperature limit of lattice heat capacity. The derived γ is 5.56(8) and 12.60(9) $\text{mJ mol}^{-1} \text{K}^{-2}$ for FeS and $\text{FeS}_{0.94}\text{Se}_{0.06}$, respectively, comparable with that of FeSe. The Debye temperature $\Theta_D = (12\pi^4 N R / 5\beta)^{1/3}$, where $N = 2$ is the number of atoms per formula unit and $R = 8.314 \text{ J mol}^{-1} \text{K}^{-1}$ is the molar gas constant. From the value of $\beta \sim 0.238(2)$ and $0.262(2) \text{ mJ mol}^{-1} \text{K}^{-3}$, we can calculate the value of Θ_D is 253.7(3) and 245.7(3) K for FeS and $\text{FeS}_{0.94}\text{Se}_{0.06}$, respectively, larger than that of FeSe (~ 210 K) [47]. According to the McMillan formula for electron-phonon mediated superconductivity, the electron-phonon coupling constant λ can be deduced

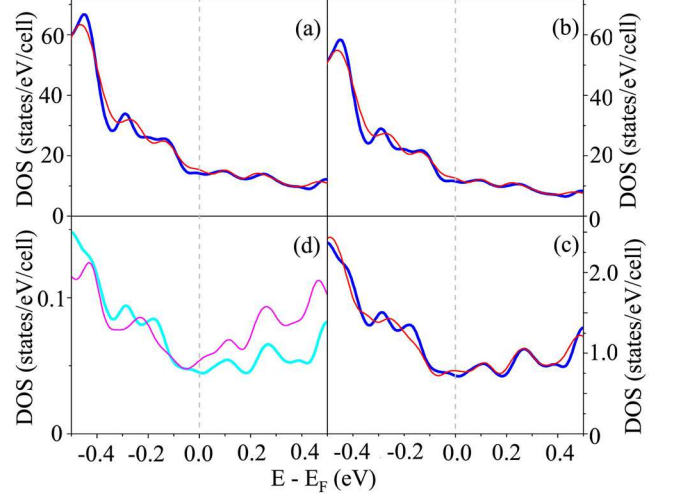


FIG. 5. (Color online) The density of states in the vicinity of the Fermi level of the tetragonal $\text{Fe}_{16}\text{S}_{16}$ supercell (blue) and the tetragonal $\text{Fe}_{16}\text{S}_{15}\text{Se}_1$ supercell (red) for: (a) Total; (b) Total Fe part; (c) Total chalcogen part; and (d) S ion in the $\text{Fe}_{16}\text{S}_{16}$ supercell (cyan) and Se ion the $\text{Fe}_{16}\text{S}_{15}\text{Se}_1$ supercell (magenta).

by

$$T_c = \frac{\Theta_D}{1.45} \exp\left[-\frac{1.04(1+\lambda)}{\lambda - \mu^*(1+0.62\lambda)}\right], \quad (4)$$

where $\mu^* \approx 0.13$ is the common value for Coulomb pseudo-potential [48]. By using the $T_c = 4.5(1)$ K and $\Theta_D = 253.7(3)$ K for FeS, we obtain $\lambda \approx 0.65(11)$, a typical value of an intermediate-coupled BCS superconductor. However, the electronic specific heat jump at T_c [Fig. 4(b)], $\Delta C_e / \gamma T_c \approx 0.43$, is much smaller than the weak coupling value of 1.43 [12, 48].

The electronic specific heat can be also expressed as:

$$\gamma = \frac{\pi^2}{2} k_B \frac{n}{T_F} = \frac{\pi^2}{3} k_B^2 N(\epsilon_F). \quad (5)$$

Combining equations (3) and (5) yields: $S/T = \pm \gamma / ne$, where the units are V K^{-1} for S , $\text{J K}^{-2} \text{m}^{-3}$ for γ , and m^{-3} for n , respectively. This relation was shown to hold in the $T = 0$ limit for a large variety of materials, even in the presence of strong correlations, including heavy fermion metals, organic conductors, and cuprates [43]. Then we can define a dimensionless quantity

$$q = \frac{S}{T} \frac{N_A e}{\gamma}, \quad (6)$$

where N_A is the Avogadro constant. The constant $N_A e = 9.6 \times 10^4 \text{ C mol}^{-1}$ is the Faraday constant. The q gives the number of carriers per formula unit (proportional to $1/n$ where n is the carrier concentration) [43]. The derived q is $\sim 2.6(1)$ for FeS, which is almost unchanged for $\text{FeS}_{0.94}\text{Se}_{0.06} \sim 2.6(2)$, in line with equivalent doping S at Se sites. Given the volume of unit

cell $\sim 0.068 \text{ nm}^3$, we obtain the carrier density per volume $n \approx 5.7(3) \times 10^{21} \text{ cm}^{-3}$ and the Fermi momentum $k_F = (3\pi^2 n)^{1/3} \approx 5.5(1) \text{ nm}^{-1}$ for FeS, which are almost unchanged with $n \approx 5.7(5) \times 10^{21} \text{ cm}^{-3}$ and $k_F \approx 5.5(2) \text{ nm}^{-1}$ for $\text{FeS}_{0.94}\text{Se}_{0.06}$, respectively. The effective mass m^* , derived from $k_B T_F = \hbar^2 k_F^2 / 2m^*$, increases from $4.8 m_e$ for FeS to $9.8 m_e$ for $\text{FeS}_{0.94}\text{Se}_{0.06}$, consistent with the increase of correlation strength with Se substitution. This confirms substantial increase in electron correlations in $\text{FeS}_{0.94}\text{Se}_{0.06}$. Furthermore, we can derive the Fermi velocity v_F using $\hbar k_F = m^* v_F$; it decreases from 133 km s^{-1} for FeS to 65 km s^{-1} for $\text{FeS}_{0.94}\text{Se}_{0.06}$.

First-principle calculations (Fig. 5) show that the Fermi level is on a pseudo-gap-like slope of the low energy side for both compounds. The density of states (DOS) in the vicinity of Fermi level for both FeS and $\text{FeS}_{0.94}\text{Se}_{0.06}$ is presented in Fig. 5(a). Partial contribution of Fe and chalcogen atoms is presented in Fig. 5(b,c); the result confirms that the Fe electronic states are dominant at the Fermi level but also that there is a small increase in partial contribution of chalcogen atoms to DOS for Se-doped crystal [Fig. 4(c)] [16, 49]. Close inspection of the region near the Fermi level for small Se substitution on S atomic site, i.e. for $\text{FeS}_{0.94}\text{S}_{0.06}$ [Fig. 5(d)] indicates increase in DOS. This confirms experimental observation but also points out that DOS changes are connected with orbital states that are partially chalcogen-derived and whose contribution is not negligible [16].

CONCLUSIONS

In summary, thermopower analysis of tetragonal FeS and $\text{FeS}_{0.94}\text{Se}_{0.06}$ indicates weak electron correlation. Both T_c/T_F and effective mass m^* substantially increase with slight Se substitution as small as 0.06. Since drastic changes in electronic structure and emergence of orbital-selective correlations associated with Lifshitz transition have been proposed to emerge with small lattice expansion in FeS [33], our results call for investigation of electronic structure in $\text{FeS}_{1-x}\text{Se}_x$ crystals.

ACKNOWLEDGEMENTS

Work at Brookhaven National Laboratory (BNL) is supported by the Office of Basic Energy Sciences, Materials Sciences and Engineering Division, U.S. Department of Energy (DOE) under Contract No. DE-SC0012704. First principle calculations were supported by the Ministry of Education, Science and Technological Development of the Republic of Serbia.

*Y.L. and A.W. contributed equally to this work.

†Present address: Los Alamos National Laboratory, Los Alamos, New Mexico 87545, USA

‡Present address: College of Physics, Chongqing Univer-

sity, Chongqing 401331, China

‡Present address: Material Science Division, Argonne National Laboratory, Lemont, Illinois 60439, USA

‡yuliu@lanl.gov

‡afwang@cqu.edu.cn

¶petrovic@bnl.gov

-
- [1] Y. Kamihara, T. Watanabe, M. Hirano, and H. Hosono, Iron-Based Layered Superconductor $\text{La}[\text{O}_{1-x}\text{F}_x]\text{FeAs}$ ($x = 0.05\text{-}0.12$) with $T_c = 26 \text{ K}$, *J. Am. Chem. Soc.* **130**, 3296 (2008).
 - [2] X. Lai, H. Zhang, Y. Wang, X. Wang, X. Zhang, J. Lin, and F. Huang, Observation of superconductivity in tetragonal FeS, *J. Am. Chem. Soc.* **137**, 10148 (2015).
 - [3] F. Hsu, J. Luo, K. Yeh, T. Chen, T. Huang, P. M. Wu, Y. Lee, Y. Huang, Y. Chu, D. Yan, and M. Wu, Superconductivity in the PbO-type structure $\alpha\text{-FeSe}$, *Proc. Natl. Acad. Sci. USA* **105**, 14262 (2008).
 - [4] U. Pachmayr, N. Fehn and D. Johrendt, Structural transition and superconductivity in hydrothermally synthesized FeX ($X = \text{S}, \text{Se}$), *Chem. Commun.* **52**, 194 (2016).
 - [5] S. J. Kuhn, M. K. Kidder, D. S. Parker, C. Cruz, M. A. McGuire, W. M. Chance, L. Li, L. Debeer-schmitt, J. Ermentrout, K. C. Littrell, M. R. Eskildsen, and A. S. Sefat, Structure and property correlations in FeS, *Physica C* **534**, 29 (2017).
 - [6] S. Hohenstein, U. Pachmayr, Z. Guguchia, S. Kamusella, R. Khasanov, A. Amato, C. Baines, H. H. Klaus, E. Morenzoni, D. Johrendt, and H. Luetkens, Coexistence of low-moment magnetism and superconductivity in tetragonal FeS and suppression of T_c under pressure, *Phys. Rev. B* **93**, 140506(R) (2016).
 - [7] J. Zhang, F. Liu, T. Ying, N. Li, Y. Xu, L. He, X. Hong, Y. Yu, M. Wang, J. Shen, W. Yang, and S. Li, Observation of two superconducting domes under pressure in tetragonal FeS, *npj Quantum Materials* **2**, 49 (2017).
 - [8] H. Man, J. Guo, R. Zhang, R. Schönemann, Z. Yin, M. Fu, M. B. Stone, Q. Huang, Y. Song, W. Wang, D. J. Singh, F. Lochner, T. Hickel, I. Eremin, L. Harriger, J. W. Lynn, C. Broholm, L. Balicas, Q. Si, and P. Dai, Spin excitations and the Fermi surface of superconducting FeS, *npj Quantum Mater.* **2**, 14 (2017).
 - [9] P. Reiss, M. D. Watson, T. K. Kim, A. A. Haghighirad, D. N. Woodruff, M. Bruma, S. J. Clarke, and A. I. Coldea, Suppression of electronic correlations by chemical pressure from FeSe to FeS, *Phys. Rev. B* **96**, 121103(R) (2017).
 - [10] X. Yang, Z. Du, G. Du, Q. Gu, H. Lin, D. Fang, H. Yang, X. Zhu, and H. H. Wen, Strong-coupling superconductivity revealed by scanning tunneling microscope in tetragonal FeS, *Phys. Rev. B* **94**, 024521 (2016).
 - [11] T. P. Ying, X. F. Lai, X. C. Hong, Y. Xu, L. P. He, J. Zhang, M. X. Wang, Y. J. Yu, F. Q. Huang, and S. Y. Li, Nodal superconductivity in FeS: Evidence from quasiparticle heat transport, *Phys. Rev. B* **94**, 100504(R) (2016).
 - [12] J. Xing, H. Lin, Y. Li, S. Li, X. Zhu, H. Yang, and H. H. Wen, Nodal superconducting gap in tetragonal FeS, *Phys. Rev. B* **93**, 104520 (2016).

- [13] C. K. H. Borg, X. Zhou, C. Eckberg, D. J. Campbell, S. R. Saha, J. Paglione, and E. E. Rodriguez, Strong anisotropy in nearly ideal tetrahedral superconducting FeS single crystals, *Phys. Rev. B* **93**, 094522 (2016).
- [14] T. Terashima, N. Kikugawa, H. Lin, X. Zhu, H. H. Wen, T. Nomoto, K. Suzuki, H. Ikeda, and S. Uji, Upper critical field and quantum oscillations in tetragonal superconducting FeS, *Phys. Rev. B* **94**, 100503(R) (2016).
- [15] H. Lin, Y. Li, Q. Deng, J. Xing, J. Liu, X. Zhu, H. Yang, and H. H. Wen, Multiband superconductivity and large anisotropy in FeS crystals, *Phys. Rev. B* **93**, 144505 (2016).
- [16] Y. Yang, W. S. Wang, H. Y. Lu, Y. Y. Xiang, and Q. H. Wang, Electronic structure and $d_{x^2-y^2}$ -wave superconductivity in FeS, *Phys. Rev. B* **93**, 104514 (2016).
- [17] A. Wang, L. Wu, V. N. Ivanovski, J. B. Warren, J. Tian, Y. Zhu, and C. Petrovic, Critical current density and vortex pinning in tetragonal $\text{FeS}_{1-x}\text{Se}_x$ ($x = 0, 0.06$), *Phys. Rev. B* **94**, 094506 (2016).
- [18] A. Wang and C. Petrovic, Vortex pinning and irreversibility fields in $\text{FeS}_{1-x}\text{Se}_x$ ($x = 0, 0.06$), *Appl. Phys. Lett.* **110**, 232601 (2017).
- [19] A. S. Sefat, M. A. McGuire, B. C. Sales, R. Jin, J. Y. Howe, and D. Mandrus, Electronic correlations in the superconductor $\text{LaFeAsO}_{0.89}\text{F}_{0.11}$ with low carrier density, *Phys. Rev. B* **77**, 174503 (2008).
- [20] N. Kang, P. Auban-Senzier, C. R. Pasquier, Z. A. Ren, J. Yang, G. C. Chen, and Z. X. Zhao, Pressure dependence of the thermoelectric power of the iron-based high- T_c superconductor $\text{SmFeAsO}_{0.85}$, *New J. Phys.* **11**, 025006 (2009).
- [21] E. D. Mun, S. L. Bud'ko, Ni Ni, A. N. Thaler, and P. C. Canfield, Thermoelectric power and Hall coefficient measurements on $\text{Ba}(\text{Fe}_{1-x}\text{T}_x)_2\text{As}_2$ ($\text{T} = \text{Co}$ and Cu), *Phys. Rev. B* **80**, 054517 (2009).
- [22] A. Pourret, L. Malone, A. B. Antunes, C. S. Yadav, P. L. Paulose, B. Fauque, and K. Behnia, Strong correlation and low carrier density in $\text{Fe}_{1+y}\text{Te}_{0.6}\text{Se}_{0.4}$ as seen from its thermoelectric response, *Phys. Rev. B* **83**, 020504(R) (2011).
- [23] M. Matusiak, T. Plackowski, Z. Bukowski, N. D. Zhigadlo, and J. Karpinski, Evidence of spin-density-wave order in $\text{RFeAsO}_{1-x}\text{F}_x$ from measurements of thermoelectric power, *Phys. Rev. B* **79**, 212502 (2009).
- [24] N. P. Butch, S. R. Saha, X.H. Zhang, K. Kirshenbaum, R. L. Greene, and J. Paglione, Effective carrier type and field dependence of the reduced- T_c superconducting state in $\text{SrFe}_{2-x}\text{Ni}_x\text{As}_2$, *Phys. Rev. B* **81**, 024518 (2010).
- [25] K. Wang, H. Lei, and C. Petrovic, Thermoelectric studies of $\text{K}_x\text{Fe}_{2-y}\text{Se}_2$ indicating a weakly correlated superconductor, *Phys. Rev. B* **83**, 174503 (2011).
- [26] K. Wang, H. Lei, and C. Petrovic, Evolution of correlation strength in $\text{K}_x\text{Fe}_{2-y}\text{Se}_2$ superconductor doped with S, *Phys. Rev. B* **84**, 054526 (2011).
- [27] C. Collignon, A. Ataei, A. Gourgout, S. Badoux, M. Lizaire, A. Legros, S. Licciardello, S. Wiedmann, J. Q. Yan, J. S. Zhou, Q. Ma, B. D. Gaulin, N. Doiron-Leyraud, and L. Tillefer, Thermopower across the phase diagram of the cuprate $\text{La}_{1.6-x}\text{Nd}_{0.4}\text{Sr}_x\text{CuO}_4$: Signatures of the pseudogap and charge density wave phases, *Phys. Rev. B* **103**, 155102 (2021).
- [28] Brian M. Andersen, Yu. S. Barash, S. Graser and P. J. Hirschfeld, Josephson effects in d -wave superconductor junctions with magnetic interlayers, *Phys. Rev. B* **77**, 054501 (2008).
- [29] F. A. Wolf, S. Graser, F. Loder, and T. Kopp, Supercurrent through Grain Boundaries of Cuprate Superconductors in the Presence of Strong Correlations, *Phys. Rev. Lett.* **108**, 117002 (2012).
- [30] Y. J. Jo, J. Jaroszynski, A. Yamamoto, A. Gurevich, S. C. Riggs, G. S. Boebinger, D. Larlabalestier, H. H. Wen, N. D. Zhigadlo, S. Katrych, Z. Bukowski, J. Karpinski, R. H. Liu, H. Chen, X. H. Chen and L. Balicas, High-field phase-diagram of Fe arsenide superconductors, *Physica C* **469**, 9 (2009).
- [31] J. Hecher, S. Ishida, D. Song, H. Ogino, A. Iyo, H. Eisaki, M. Nakajima, D. Kagerbauer and M. Eisterer, Direct observation of in-plane anisotropy of the superconducting critical current density in $\text{Ba}(\text{Fe}_{1-x}\text{Co}_x)_2\text{As}_2$ crystals, *Phys. Rev. B* **97**, 014511 (2018).
- [32] Shun-Li Yu, Jing Kang and Jian-Xin Li, Band renormalization and Fermi surface reconstruction in iron-based superconductors, *Phys. Rev. B* **79**, 064517 (2009).
- [33] S. L. Skornyakov and I. Leonov, Correlated electronic structure, orbital-dependent correlations, and Lifshitz transition in tetragonal FeS, *Phys. Rev. B* **100**, 235123 (2019).
- [34] G. Kresse and J. Furthmüller, Efficient iterative schemes for *ab-initio* total-energy calculations using a plane-wave basis set, *Phys. Rev. B* **54**, 11169 (1996).
- [35] C. H. Lee, K. Kihou, A. Iyo, H. Kito, P. M. Shirage, and H. Eisaki, Relationship between crystal structure and superconductivity in iron-based superconductors, *Solid State Commun.* **152**, 644 (2012).
- [36] R. A. Smith, *Semiconductor* (Cambridge: Cambridge University Press, 1978).
- [37] Y. J. Song, J. B. Hong, B. H. Min, and Y. S. Kwon, Superconducting properties of a stoichiometric FeSe compound and two anomalous features in the normal state, *J. Korean Phys. Soc.* **59**, 312 (2011).
- [38] F. Caglieris, F. Ricci, G. Lamura, A. Martinelli, A. Palenzona, I. Pallecchi, A. Sala, G. Profeta, and M. Putti, Theoretical and experimental investigation of magnetotransport in iron chalcogenides, *Sci. Technol. Adv. Mater.* **13**, 054402 (2012).
- [39] I. Pallecchi, F. Caglieris, and M. Putti, Thermoelectric properties of iron-based superconductors and parent compounds, *Supercond. Sci. Technol.* **29**, 073002 (2016).
- [40] A. Subedi, L. Zhang, D. J. Singh, and M. H. Du, Density functional study of FeS, FeSe, and FeTe: Electronic structure, magnetism, phonons, and superconductivity, *Phys. Rev. B* **78**, 134514 (2008).
- [41] R. D. Barnard, *Thermoelectricity in Metals and Alloys* (Taylor & Francis, London, 1972).
- [42] J. L. Cohn, S. A. Wolf, V. Selvamanickam, and K. Salama, Thermoelectric power of $\text{YBa}_2\text{Cu}_3\text{O}_{7-\delta}$: Phonon drag and multiband conduction, *Phys. Rev. Lett.* **66**, 1098 (1991).
- [43] K. Behnia, D. Jaccard and J. Flouquet, On the thermoelectricity of correlated electrons in the zero-temperature limit, *J. Phys.: Condens. Matter.* **16**, 5187 (2004).
- [44] K. Miyake and H. Kohno, Theory of Quasi-Universal Ratio of Seebeck Coefficient to Specific Heat in Zero-Temperature Limit in Correlated Metals, *J. Phys. Soc. Jpn.* **74**, 254 (2005).
- [45] J. L. Sarrao and J. D. Thompson, Superconductivity in Cerium- and Plutonium-Based '115' Materials, *J. Phys. Soc. Jpn.* **76**, 051013 (2007).

- [46] T. Moriya and K. Uedo, Antiferromagnetic spinfluctuation and superconductivity, *Rep. Prog. Phys.* **66**, 1299 (2003).
- [47] J. Y. Lin, Y. S. Hsieh, D. A. Chareev, A. N. Vasiliev, Y. Parsons, and H. D. Yang, Coexistence of isotropic and extended s -wave order parameters in FeSe as revealed by low-temperature specific heat, *Phys. Rev. B* **84**, 220507(R) (2011).
- [48] W. L. McMillan, Transition Temperature of Strong-Coupled Superconductors, *Phys. Rev.* **167**, 331 (1968).
- [49] J. Miao, X. H. Niu, D. F. Xu, Q. Yao, Q. Y. Chen, T. P. Ying, S. Y. Li, Y. F. Fang, J. C. Zhang, S. Ideta, K. Tanaka, B. P. Xie, D. L. Feng, and Fei Chen, Electronic structure of FeS, *Phys. Rev. B* **95**, 205127 (2017).